Research
Biomedical Engineering—Article

A Temporal–Spatial Atlas of Peripheral Nerve Evoked Cortex Potential in Rat: A Novel Testbed to Explore the Responding Patterns of the Brain to Peripheral Nerves

Xiaofeng Yin [*,#], Jiuxu Deng [#], Bo Chen, Bo Jin, Xinyi Gu, Zhidan Qi, Kunpeng Leng, Baoguo Jiang [*]

Department of Trauma and Orthopedics, Peking University People's Hospital, Beijing 100044, China

ARTICLE INFO

ABSTRACT

Observing the dynamic progress of the brain in response to peripheral nerve stimulation as a whole is the basis for a deeper understanding of overall brain function; however, it remains a great challenge. In this work, a novel mini-invasive orthogonal recording method is developed to observe the overall evoked cortex potential (ECP) in rat brain. A typical ECP atlas with recognizable waveforms in the rat cortex corresponding to the median, ulnar, and radial nerve trunks and subdivided branches is acquired. Reproducible exciting temporal–spatial progress in the rat brain is obtained and visualized for the first time. Changes in the ECPs and exciting sequences in the cortex four months after median nerve transection are also observed. The results suggest that the brain's response to peripheral stimulation has precise and reproducible temporal–spatial properties. This resource can serve as a testbed to explore the overall functional interaction and dynamic remodeling mechanisms between the peripheral and central nervous systems over time.

© 2021 THE AUTHORS. Published by Elsevier LTD on behalf of Chinese Academy of Engineering and Higher Education Press Limited Company. This is an open access article under the CC BY-NC-ND license (http://creativecommons.org/licenses/by-nc-nd/4.0/).

1. Introduction

Brain electrical activity—that is, the excitement of neurons—is an important reflection of brain function [1–7]. Continuously observing the electrophysiological signals in the brain is important for understanding the function and message-processing mechanisms of the nervous system [8–20]. The electrical response of the brain to stimulation has been well studied in isolated areas of the cortex or in a small number of neurons (e.g., the evoked cortex potential (ECP), which can be recorded by a multi-electrode matrixes); however, little is known of the exact temporal–spatial progress of the brain's reaction to peripheral nerve stimulation. This is a critical knowledge gap, because brain function is accomplished by the coordination of numerous neurons and nuclei. Such complicated process cannot be well understood with the fragmental information on the nervous system obtained by traditional methods. However, determining the functional parameters of the

brain as completely as possible is extremely challenging, given the shortcomings of traditional ECP-recording methods based on a single electrode or multi-electrode matrix [21–23]. First, recorded signals only reflect the action potential of a few cortical neurons around the electrode [24,25]. Therefore, it is difficult to obtain the electrophysiological characteristics of whole cell populations in the target regions and analyze complicated brain functions. Second, a slight change in electrode position results in a major fluctuation in the signals as well as significant individual variations, which makes it easy to miss the common regularities. Third, traditional craniotomy and placing electrodes onto the surface of the cortex or into the cortex result in severe trauma and extensive disturbance to the brain. Moreover, it is difficult to achieve long-term, continuous observation using traditional methods. Therefore, grasping the dynamic temporal–spatial progress of the brain in response to the stimulation of peripheral nerves can be extremely useful in obtaining a deeper understanding of the working patterns of the brain.

In this research, we develop a novel electrophysiological method with an orthogonal lead system and mini-invasive procedures, and investigate the overall excitation progress in different brain functional regions corresponding to peripheral stimulations

* Corresponding authors.
    E-mail addresses: xiaofengyin@bjmu.edu.cn (X. Yin), jiangbaoguo@vip.sina.com (B. Jiang).
    # These authors contributed equally to this work.

in rats. We also provide a fully typical ECP atlas of different peripheral nerves and their subdivided branches, making it possible to visualize the temporal–spatial properties and interactions of the brain and peripheral nerve reconstructions.

2. Methods

2.1. Description of animals and ethics statement

Adult male Sprague–Dawley rats weighing 200–250 g were acquired from the Laboratory Animal Center of Peking University People's Hospital (PKUPH; specific pathogen free level, animal use permit No. SYXK (jing) 2011-0010). The rats were maintained on a 12 h light/dark cycle with free access to pellet food and water. The anesthetic, surgical, and postoperative care protocols used in this research conformed to the National Institutes of Health guidelines regarding animal experimentation and were approved by the Research Ethics Committee at PKUPH. Every effort was made to minimize animal suffering and reduce the number of animals used.

2.2. Surgical procedures and electrode implantation

Rats were randomly separated into groups to test the ECPs of the median, ulnar, and radial nerves and branches separately. For the three main forearm nerve trunks, 18 animals were used to obtain the electrical signals (six animals for one nerve). For the branches of the three nerve trunks, another 18 animals were used to obtain data and avoid unnecessary reaction errors in the rats due to different operation planes and a long operation time.

The rats were anesthetized using sodium pentobarbital with a dosage of 30 mg·kg^{-1} via intraperitoneal injection; they were also given 15 mg·kg^{-1} sodium pentobarbital to maintain the depth of the anesthesia when necessary. The head and right limbs were shaved and sterilized. The trunks and subdivided branches of the median, ulnar, and radial nerves were exposed from the surrounding tissues and moistened by infiltration with saline gauze. The room temperature was maintained at 20–25 °C while the experiment was performed. A homeothermic blanket system was used to maintain the rectal temperature at 37.0–37.5 °C and to prevent hypothermia, which may affect the physiological activity of the brain.

The rat head was fixed in a stereotaxic instrument. An approximately 3 cm long midline incision was made. After adequate exposure of the operation region from the lambda to the bregma, 3% hydrogen peroxide was used to clean the skull surface. As reported by Khazipov et al. [26] and Paxinos et al. [27], the electrode positions A1, A2, B1, and B2 were identified (Figs. 1(a) and (b)). Ag/AgCl pins (head size of 8 mm, wall thickness of 0.2 mm, inner diameter of 0.5 mm, tail length of 1 mm, and diameter of 0.5 mm) were used as recording electrodes and were inserted into the marked points on the skull surface (diameter of 0.5 mm and depth of 1 mm) (Figs. 1(b) and (c)). Our method skillfully avoided the location of sinusoids in order to reduce the possibility of accidental injury of the blood sinus causing intracranial hematoma.

2.3. Evoked cortex potentials recording

The target nerve and its branches were carefully exposed. An electrical stimulator (MedlecSynergy; Oxford Instrument Inc., UK) was set to the designed position using bipolar electrodes. Spherical Ag/AgCl electrodes were used to collect the cortical signals. The line connecting A1 to A2 was set as the horizontal (H) lead, while the line connecting B1 to B2 was set as the vertical (V) lead. The stimulus intensity was 0.09 mA, the duration was 0.2 ms, and the repetition rate was 5 pulse per second (pps). A monophasic square-wave constant current pattern (3 Hz, 100 μs pulse width) was used. On average, 300 sweeps were used for the acquisition of one ECP trace. To illustrate the waveform of the ECP, we marked the negative wave as N, and the positive wave as P. If the amplitude was higher than 10 μV, the waveform was marked as N or P. Otherwise, the waveform was marked as n or p. ECPs were recorded by stimulating the median, ulnar, and radial nerves and their subdivided branches, respectively.

2.4. Temporal–spatial parameters conversion from an orthogonal lead system

In a rectangular coordinate system, the positive direction of the horizontal ECP vector $\mathbf{x}$ points from A1 to A2, while the positive direction of the vertical ECP vector $\mathbf{y}$ points from B2 to B1. The resultant ECP vector $\boldsymbol{\rho}$ is synthesized by the horizontal and vertical components. To better understand the temporal–spatial character of the ECP, we converted the rectangular coordinate system into a polar coordinate system, where point o was the intersection of vector $\mathbf{x}$ and vector $\mathbf{y}$, $\boldsymbol{\rho} = \sqrt{\mathbf{x}^2 + \mathbf{y}^2}$ and $\theta = \tan^{-1}(\mathbf{x}, \mathbf{y})$, which was intersection angle from ox to $\boldsymbol{\rho}$. Time (t) was set as another parameter in the polar coordinate system. Thus, ECP = $(\boldsymbol{\rho}, \theta, t)$.
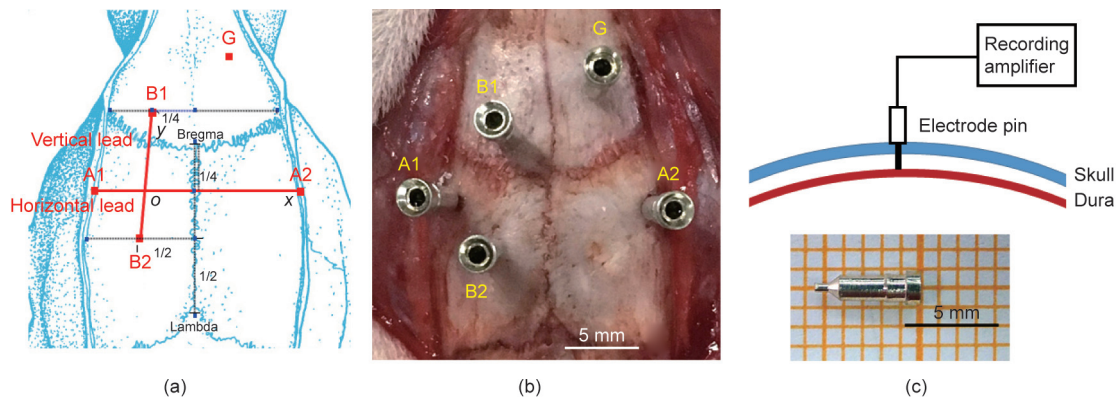
Fig. 1. (a) Using the bregma and lambda as references to determine the electrode positions at A1, A2, B1, and B2. The horizontal lead is the line connecting A1 and A2; the vertical lead is the line connecting B1 and B2. (b) Orthogonal lead system in rat. (c) Pins were used as the recording electrodes. The electrodes are just broken through the skull diploe and are exposed to the dura; the cerebral cortex still remains intact. G is the ground point.

2.5. Median nerve transection model

A total of six rats were anesthetized with 30 mg·kg^{-1} of pentobarbital sodium by intraperitoneal injection. The operation sites were shaved and sterilized, followed by decortication. After being exposed, the median nerve was transected at 3 mm above the cubital fossa. The proximal stump of the median nerve was ligated with 5-0 nylon sutures and stitched to the adjacent muscle in the reverse direction to prevent nerve growth. The wound was rinsed with sufficient saline and then closed with 5-0 nylon sutures. The rats were placed back into the cages. Electrophysiological examinations were performed four months after the operation to assess the change in ECP.

2.6. Data analysis

Data in this work are expressed as the mean ± standard deviation (SD). Analysis and statistics were performed using SPSS 20.0 software (SPSS Inc., USA).

3. Results

3.1. The position relationship between the electrode and the cortical functional areas in rat

In this experiment, the orthogonal lead was located above the somatic motor and the somatosensory region in the left brain. The green and red areas in Fig. 2 represent the somatic motor and the somatosensory area, respectively; the H lead and V lead orthogonally cross through the corresponding cortical functional areas.

3.2. Temporal–spatial characteristics of ECPs induced by the median nerve and its subdivided branches

Stable ECPs can be obtained in both the H lead and the V lead by stimulating the median nerve trunk. The latency of the ECP in the H and V leads was (1.21 ± 0.04) and (1.25 ± 0.06) ms, respectively, which was in accordance with the time required for the nerve
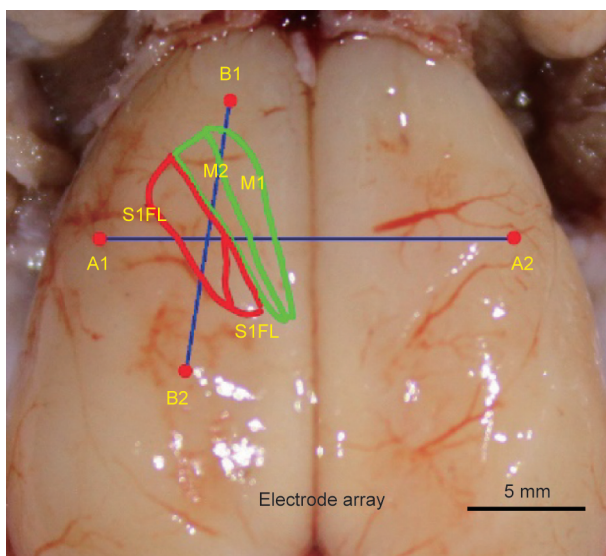
Fig. 2. Relationship between the orthogonal lead and the cortical functional areas. A schematic diagram of the functional areas in the rat cortex. The green and red areas represent the somatic motor and the somatosensory area, respectively. S1FL: primary somatosensory cortex forelimb region; S1HL: primary somatosensory cortex hindlimb region; M1: primary motor cortex; M2: secondary motor cortex.

pulse to spread from the stimulated site to the cortex (Fig. 3 and Table 1).

The main ECP wave of the median nerve trunk in the H lead consisted of four consecutive negative waves ($n_1N_2N_3N_4$). The main ECP in the V lead showed a waveform of the $N_1N_2n_3$ type (Fig. 3 and Table 2).

The ECPs induced by the median nerve branches (i.e., the muscular branch, anterior interosseous nerve, radial side common palmar digital nerve, median side common palmar digital nerve, and ulnar side common palmar digital nerve) had their own characteristics and could be recognized through specific waveforms (Figs. 3(a) and (b) and Table 1).

In the polar coordinate system, the exciting temporal–spatial sequences of the cortex corresponding to the stimulations of different nerve branches were acquired. For the median nerve trunk, the exciting projection region started from the second quadrant in the first 12.5 ms (ranging from nearly 225° to 240°), which was equivalent to the primary motor cortex (M1) edge. During the next 12.5 ms, the activation area moved to the region ranging from approximately 210° to 225°. Finally, after clockwise spreading, the projection region ended in the first quadrant (87.5–100.0 ms range from nearly 45° to 60°), which corresponded to the secondary motor cortex (M2) edge (Fig. 3(c)). The exciting processes of the cortex induced by different median nerve branches exhibited specific temporal–spatial characteristics (Figs. 3(b) and (c)).

3.3. Temporal–spatial characteristics of ECPs induced by the ulnar nerve and its subdivided branches

The latencies in the H and V leads of the ulnar nerve trunk were respectively (1.30 ± 0.06) and (1.25 ± 0.04) ms (Fig. 4 and Table 3). Unlike the median nerve, the main ECP wave of the ulnar nerve trunk in the H lead presented as the n_1N_2 type, consisting of a plateau between the two consecutive negative waves (n_1 and N_2). The main ECP wave in the V lead was the $n_1p_1N_2$ type (Fig. 4 and Table 4).

When branches of the ulnar nerve (i.e., two dorsal digital nerves and two cutaneous branches) were stimulated, the ECP waveforms in the H lead all presented as N type, while those in the V lead exhibited a complex type (Fig. 4 and Table 3).

The ECP vector of the ulnar nerve trunk started from the area between the second and the first quadrants in the first 12.5 ms (around 170° to 210°), which was the edge of the M1. In the next 12.5 ms, the activating area moved to both sides of the initial exciting region from approximately 225° to 250° and from 150° to 170°. Finally, after bidirectional spread, the exciting region ended in the first quadrant (30° to 65°), which corresponded to the M2 edge (Fig. 4(c)). The exciting processes of the cortex areas corresponding to each branched ulnar nerve exhibited different temporal–spatial characteristics (Fig. 4(c)).

3.4. Temporal–spatial characteristics of ECPs induced by the radial nerve and its subdivided branches

The latencies of the ECP in the H and V leads of the radial nerve trunk were respectively (1.28 ± 0.05) and (1.30 ± 0.06) ms (Table 5). The main ECP wave of the radial nerve trunk in the H lead began with a remarkable positive wave (P_1), followed by three consecutive negative waves ($P_1N_1N_2N_3$). The main ECP waveform in the V lead was of the $n_1p_1N_2$ type. (Figs. 5(a) and (b) and Table 6). Most of the ECPs induced by the branches of the radial nerve in the H lead (i.e., the triceps long head muscle branch, triceps lateral head muscle branch, radialis profundus, and radialis superficialis) had a distinct initial positive wave (Table 5).

The exciting spatial distribution in the cortex induced by the radial nerve trunk was shaped like a rectangle. It started from
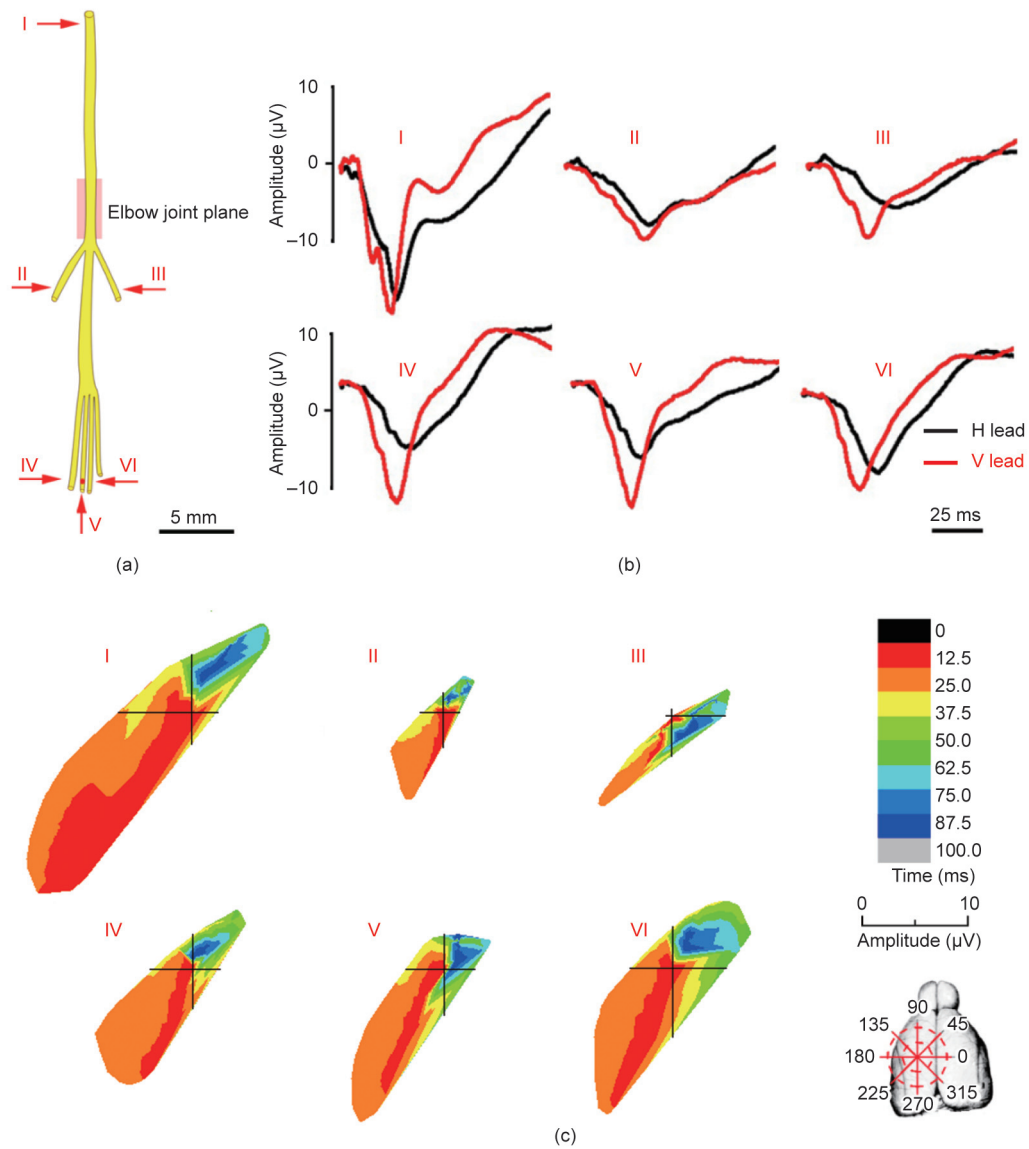
Fig. 3. ECPs induced by the median nerve and its subdivided branches. (a) Sketch map of the median nerve and arrows indicate the stimulating points. (b) The ECP waveform of the median nerve and its subdivided branches. (c) The temporal–spatial characteristics of the ECP induced by the median nerve and its subdivided branches. I: Median nerve; II: muscular branch of the median nerve; III: anterior interosseous nerve; IV–VI: common palmar digital nerves (radial, median, and ulnar side, respectively).

Table 1
Parameters of the ECPs induced by the median nerve and its subdivided branches (mean ± SD, $n = 6$).

Parameter	Median nerve	Muscular branch	Anterior interosseous nerve	Common palmar digital nerve (radial)	Common palmar digital nerve (median)	Common palmar digital nerve (ulnar)
Waveform						
H lead	$n_1N_2N_3$	p_1N_1	$p_1N_1N_2$	N	n_1N_2	N_1N_2
V lead	$N_1N_2n_3$	N_1N_2	N_1n_2	N	N	N_1N_2
Latency						
H lead (ms)	1.21 ± 0.04	1.29 ± 0.04	1.30 ± 0.07	1.40 ± 0.05	1.45 ± 0.04	1.45 ± 0.06
V lead (ms)	1.25 ± 0.06	1.30 ± 0.04	1.29 ± 0.09	1.45 ± 0.10	1.50 ± 0.10	1.50 ± 0.03

Table 2
Parameters of the main ECP waveform of the median nerve trunk in the H and V leads (mean ± SD, $n = 6$).

Parameter	H lead				V lead		
	n_1	N_2	N_3	N_4	N_1	N_2	n_3
Amplitude (μV)	1.80 ± 1.20	8.37 ± 5.01	14.51 ± 9.43	8.12 ± 5.35	12.68 ± 10.70	24.96 ± 19.38	6.31 ± 4.96
Peak time (ms)	3.11 ± 0.44	8.38 ± 1.15	12.64 ± 2.35	30.46 ± 6.82	7.22 ± 2.74	10.67 ± 1.94	23.79 ± 1.77
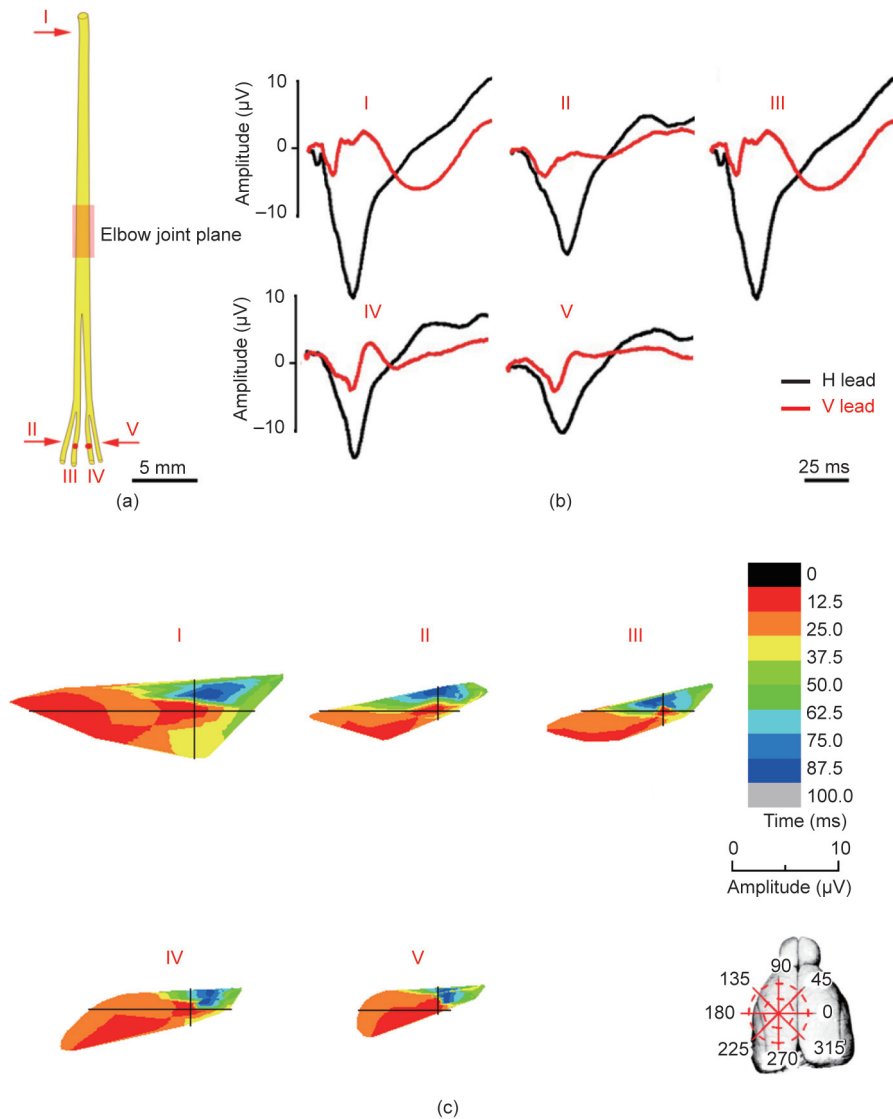
Fig. 4. ECPs induced by the ulnar nerve and its subdivided branches. (a) Sketch map of the ulnar nerve and arrows indicate the stimulating points. (b) The ECP waveform of the ulnar nerve and its subdivided branches. (c) The temporal–spatial characteristics of the ECP induced by the ulnar nerve and its subdivided branches. I: Ulnar nerve; II and III: dorsal digital nerves (radial and ulnar side, respectively); IV and V: cutaneous branches (radial and ulnar side, respectively).

Table 3
Parameters of the ECPs induced by the ulnar nerve and its subdivided branches (mean ± SD, $n = 6$).

Parameter	Ulnar nerve	Dorsal digital nerve (radial)	Dorsal digital nerve (ulnar)	Cutaneous branch (radial)	Cutaneous branch (ulnar)
Waveform					
H lead	n_1N_2	N	N	N	N
V lead	$n_1p_1N_2$	n_1n_2	n_1n_2	$N_1p_1n_2$	n
Latency					
H lead (ms)	1.30 ± 0.06	1.35 ± 0.07	1.55 ± 0.06	1.51 ± 0.06	1.53 ± 0.08
V lead (ms)	1.25 ± 0.04	1.36 ± 0.06	1.50 ± 0.12	1.55 ± 0.07	1.52 ± 0.03

Table 4
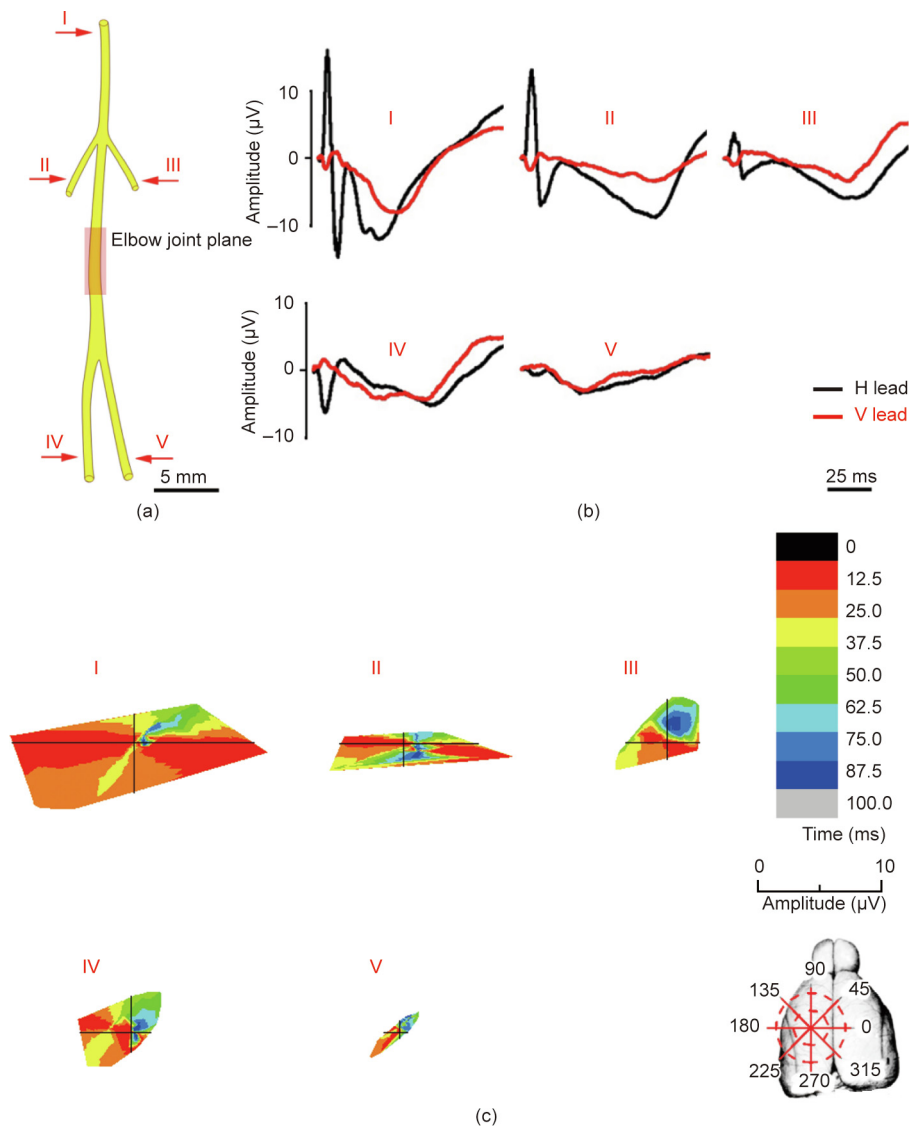Parameters of main ECP waveform of the ulnar nerve trunk in the H and V leads (mean ± SD, $n = 6$).

Parameter	H lead		V lead		
	n_1	N_2	n_1	p_1	N_2
Amplitude (µV)	3.23 ± 0.79	27.47 ± 12.51	11.55 ± 11.54	−9.94 ± 8.37	8.47 ± 8.96
Peak time (ms)	2.86 ± 0.39	12.76 ± 1.89	7.94 ± 2.77	13.53 ± 4.57	30.87 ± 4.78

the top and bottom areas of the original site in the first 12.5 ms (from 170° to 210° and from 310° to 360°), which was close to the edge of the M1. During the next 12.5 ms, the ECP signal spread to both sides next to the initial exciting region (from approximately 210° to 300° and small area near 160° and 10°). Finally, after bidirectional spread, the excitatory signal ended in the first

Table 5
Parameters of the ECPs induced by the radial nerve and its subdivided branches (mean ± SD, $n = 6$).

Parameter	Radial nerve	Triceps long head muscle branch	Triceps lateral head muscle branch	Radialis profundus	Radialis superficialis
Waveform					
H lead	$P_1N_1N_2N_3$	$P_1N_1N_2$	$p_1n_1N_2$	$N_1p_1N_2$	n_1n_2
V lead	$n_1p_1N_2$	$n_1p_1n_2n_3$	$n_1p_1n_2$	$p_1n_1n_2$	n
Latency					
H lead (ms)	1.28 ± 0.05	1.29 ± 0.06	1.30 ± 0.06	1.49 ± 0.07	1.46 ± 0.06
V lead (ms)	1.30 ± 0.06	1.31 ± 0.03	1.29 ± 0.07	1.47 ± 0.04	1.50 ± 0.08

Fig. 5. ECPs induced by the radial nerve and its subdivided branches. (a) Sketch map of the radial nerve and arrows indicate the stimulating points. (b) The ECP waveform of the radial nerve and its subdivided branches. (c) Temporal–spatial sequences analysis of the radial nerve and its subdivided branches in the orthogonal lead system. I: Radial nerve; II: branch to the long head of the triceps muscle of the radial nerve; III: branch to the lateral head of the triceps muscle of the radial nerve; IV: radialis profundus; V: radialis superficialis.

Table 6
Parameters of main ECP waveform of the radial nerve trunk in the H and V leads (mean ± SD, $n = 6$).

Parameter	H lead				V lead		
	P_1	N_1	N_2	N_3	n_1	p_1	N_2
Amplitude (µV)	−16.32 ± 9.32	18.60 ± 10.06	10.18 ± 10.65	11.60 ± 14.92	1.90 ± 1.93	−2.38 ± 0.99	10.40 ± 6.98
Peak time (ms)	2.59 ± 0.39	5.16 ± 0.80	13.07 ± 0.91	22.28 ± 3.01	2.59 ± 0.42	4.69 ± 0.84	22.06 ± 3.00

quadrant (from nearly 30° to 60°, at the M2) (Fig. 5(c)). The exciting processes of the cortex areas corresponding to each radial nerve branch exhibited specific temporal–spatial characteristics (Fig. 5(c)).

3.5. ECP temporal–spatial change after median nerve damage

Upon re-examination four months after the median nerve transection, significant changes occurred in the temporal–spatial characteristics and waveforms of the ECPs when stimulating the ulnar and radial nerve trunks using the same method as before. The main ECP waveform of the ulnar nerve trunk in the H lead changed into the $n_1N_2N_3$ type, compared with the n_1N_2 type in normal rats. In the V lead, it changed into the N_1N_2 type, compared with the initial $n_1p_1N_2$ type (Table 7). For the radial nerve, the ECP waveforms in the H and V leads became $P_1N_1N_2$ and $n_1p_1n_2$, respectively, in comparison with $P_1N_1N_2N_3$ and $n_1p_1N_2$, respectively, before the operation (Table 8).

Although the shape of the excitatory region evoked by the ulnar nerve four months after the operation remained triangular, the distribution area showed a tendency to extend to the median nerve evoked regions. The distribution area started from the third quadrant in the first 12.5 ms (from 235° to 250°, at the M1). In the following 12.5 ms, the excitatory area moved anti-clockwise to the areas (approximately 225° to 230°). Finally, after clockwise spreading, the excitatory region ended in a small area at the first and second quadrants (330° to 360° and 0 to 30°), which corresponded to

the M2 (Fig. 6). For the radial nerve, the excitation progress retained its original pattern. However, the amplitude of the ECP vectors increased significantly after the median nerve injury (Fig. 7).

4. Discussion

In this research, we developed a novel electrophysiological method with an orthogonal lead system and mini-invasive procedures that can acquire the resultant ECPs and temporal–spatial sequences in response to stimulations of peripheral nerves. A ten-year brain research plan was recently proposed by the United States' government to overcome limitations in brain research caused by fragmental knowledge of the nervous system [28–31]. In that plan, an important research field is the development of new techniques in order to understand complex brain functions in as integral a way as possible [30,32,33]. Traditional electrophysiological methods can only measure the nerve conduction velocity and the evoked potentials to determine the continuity between peripheral nerves and the brain [34]. It is difficult to monitor and analyze the complicated functional relationship between the peripheral and central nervous systems. The method developed herein provides a way to continuously capture the overall ECP signals corresponding to stimulations of the peripheral nerves. These complicated signals are then decomposed into multiple orthogonal spaces, so that the resultant brain electrical signals can be extensively analyzed into time and space components. In this way, the
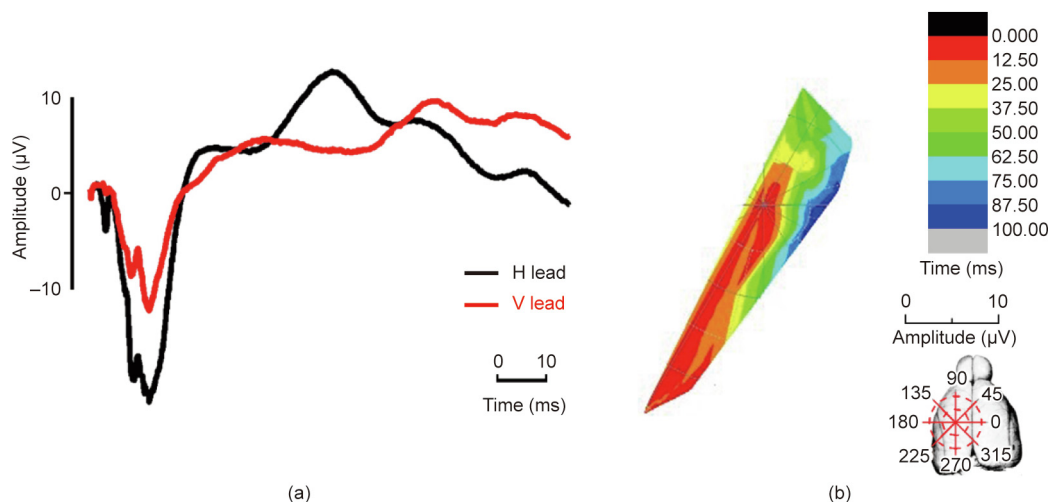
Table 7
Waveforms and latency time of the ulnar nerve trunk after median nerve transection (mean ± SD, $n = 6$).

Parameter	H lead			V lead	
	n_1	N_2	N_3	N_1	N_2
Amplitude (µV)	6.47 ± 5.06	30.24 ± 18.65	52.34 ± 43.06	12.21 ± 6.91	14.83 ± 10.55
Peak time (ms)	2.92 ± 0.35	8.34 ± 0.94	12.40 ± 1.69	8.16 ± 0.88	14.16 ± 2.17

Table 8
Waveform and latency time of the radial nerve trunk after median nerve transection (mean ± SD, $n = 6$).

Parameter	H lead			V lead		
	P_1	N_1	N_2	n_1	p_1	n_2
Amplitude (µV)	−21.56 ± 14.43	31.03 ± 19.48	60.60 ± 53.51	9.32 ± 6.29	−5.40 ± 6.06	7.29 ± 4.46
Peak time (ms)	2.76 ± 1.11	6.64 ± 2.85	13.14 ± 1.68	3.36 ± 0.54	4.78 ± 0.39	13.91 ± 3.18

Fig. 6. Temporal–spatial change of the ECP induced by the ulnar nerve four months after median nerve transection. (a) The ECP waveform and (b) temporal–spatial sequences of the ulnar nerve.
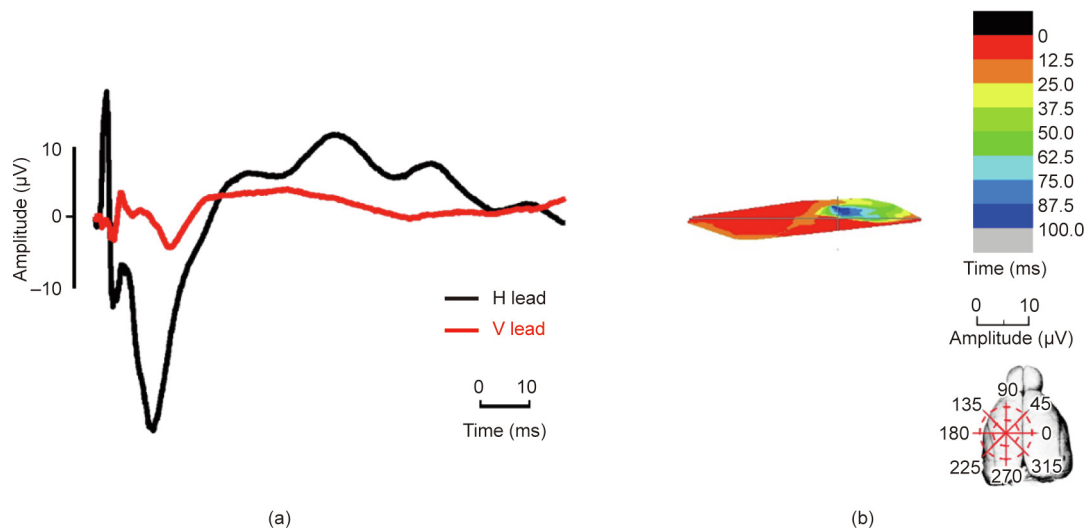
Fig. 7. Temporal–spatial change of the ECP induced by the radial nerve four months after median nerve transection. (a) The ECP waveform and (b) temporal–spatial sequences of the radial nerve.

functional states of multiple brain cortical regions in different phases could be viewed by the researchers. Our work significantly overcomes the inevitable defects in traditional methods such as poor stability and reproducibility, serious individual variation, and limited representation; thus, the present study represents a great step forward in reflecting the overall functional processes and characteristics of the brain.

A typical ECP atlas corresponding to the different peripheral nerves and subdivided branches was first obtained using the method presented herein. According to the ECP atlas results, a peripheral nerve or branch can easily be distinguished by its typical waveform. As described in the results, stimulation of the radial nerve evoked three consecutive negative waves following a large amplitude pre-phase positive wave in the H lead ($P_1N_1N_2N_3$), while the ECP of the ulnar nerve consisted of a small negative wave following a deep negative wave with a small slope in the H lead (n_1N_2). Similar results were observed in the other small nerve branches. Moreover, the parameters of the ECP, such as latency time, amplitude, and wave composition, were highly relative to the states of neural function such as nerve conductive velocity, exciting degrees, and distribution of activated cellular populations (Fig. 8). Therefore, it was possible to analyze the characteristics of

Fig. 8. A theoretical model diagram of the ECP evoked by stimulation of the radial nerve. The ECP induced by a specific nerve stimulation exhibits distinguished and repeatable parameter characteristics, including latency time, amplitude, and wave composition.

the waveform, and then determine the status and interaction between the peripheral nerve and the brain cortex. This method is similar to the use of an electrocardiogram to interpret the working status of the heart. Thus, the highly recognizable ECP atlas can be used to analyze advanced brain functions.

The method described above allowed us to visualize the temporal–spatial properties and the precise progress of the brain in response to specific peripheral nerve stimulation and reconstruction. According to our results, the ECP vectors of the median nerve are mainly located in the M1 and lateral M2. Furthermore, the detailed excitation progress from the lateral M1 spreading clockwise to the M1/M2 border was captured and visualized step by step in time and space. The excitation progress in the cortex of the radial and ulnar nerves and their branches was also represented herein. When the brain performs an action, different sets of neurons depolarize, repolarize, or have their membrane potential changed in a coordinate manner. The location and time phase of the ECP vectors projected in the orthogonal plane indicated the space distributions of different functional cell populations in the brain cortex and the time sequences of the relevant neuron groups involved in the reaction. Therefore, this method allowed the researchers to precisely observe and analyze the detailed exciting space–time sequences of the brain visually.

Major discoveries in scientific analysis—such as the ECP atlas and visualizations of exciting sequences in the cortex in response to peripheral stimulations reported here—are primarily useful for obtaining an understanding of the working programs and reaction patterns of the brain and for generating new hypotheses. The results obtained by the method presented here have generated a number of clues to be investigated in future studies. The observed exciting sequences of the projected cortex areas specific to different nerves indicate complex neuro signal transferring progresses and responding mechanisms in the brain. The data described here provide a basis for power analyses for subsequent studies, and the ECP atlas provided here can serve as a baseline reference for other researches. Variations in the ECP waves and temporal–spatial sequences would then suggest typical pathological and physiological processes in nerve function change and brain remodeling. As shown in Figs. 6 and 7, the tendency of ECPs extending to the median nerve projection areas was observed in the cortex after median nerve transection. More detailed progress could be examined in greater depth.
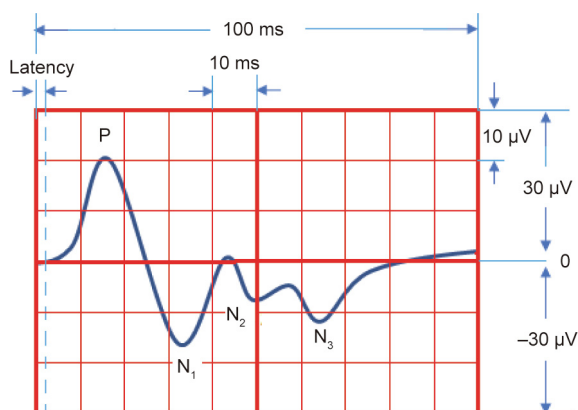
In conclusion, this study provides a novel method for exploring the overall functional connection and remodeling mechanisms between the peripheral and central nervous systems. The precise and reproducible temporal–spatial response of the brain to peripheral stimulation has been obtained for the first time. This method is simple and stable with excellent reproducibility and trivial individual variations. It provides a wealth of information and a basis for systematic analyses of the functional connections between the peripheral and central nervous systems. This resource can serve as a testbed to study the dynamic interactions of the brain and peripheral nerve reconstructions over time. However, there is a lack of exact analyses of the physiological meaning of each wave component. The parameters obtained in this study were all obtained under anesthesia; although the stimulation of each peripheral nerve showed a unique repetitive brain feedback waveform, these should be different from those in a normal physiological state. Future studies will address these problems in more detail.

Acknowledgments

Compliance with ethics guidelines

Xiaofeng Yin, Jiuxu Deng, Bo Chen, Bo Jin, Xinyi Gu, Zhidan Qi, Kunpeng Leng, and Baoguo Jiang declare that they have no conflict of interest or financial conflicts to disclose.

References

[1] Alivisatos AP, Chun M, Church G, Greenspan R, Roukes M, Yuste R. The brain activity map project and the challenge of functional connectomics. Neuron 2012;74(6):970–4.
[2] Bekhtereva NP. Certain general physiological principles of human brain functioning. Fiziol Cheloveka 1986;12(5):817–30. Russian.
[3] Birbaumer N. Brain–computer-interface research: coming of age. Clin Neurophysiol 2006;117(3):479–83.
[4] Donoghue JP. Connecting cortex to machines: recent advances in brain interfaces. Nat Neurosci 2002;5(S11):1085–8.
[5] Fox MD, Raichle ME. Spontaneous fluctuations in brain activity observed with functional magnetic resonance imaging. Nat Rev Neurosci 2007;8(9):700–11.
[6] Kempermann G, Gage FH. New nerve cells for the adult brain. Sci Am 1999;280 (5):48–53.
[7] Kempermann G, Kuhn HG, Winkler J, Gage FH. New nerve cells for the adult brain. Adult neurogenesis and stem cell concepts in neurologic research. Nervenarzt 1998;69(10):851–7. German.
[8] Albanese SA, Spadaro JA, Lubicky JP, Henderson NA. Somatosensory cortical evoked potential changes after deformity correction. Spine 1991;16(8 Suppl): S371–4.
[9] Allison T, McCarthy G, Luby M, Puce A, Spencer DD. Localization of functional regions of human mesial cortex by somatosensory evoked potential recording and by cortical stimulation. Electroencephalogr Clin Neurophysiol 1996;100 (2):126–40.
[10] Bai X, Towle VL, van Drongelen W, He B. Cortical potential imaging of somatosensory evoked potentials by means of the boundary element method in pediatric epilepsy patients. Brain Topogr 2011;23(4):333–43.
[11] Custead R, Oh H, Rosner AO, Barlow S. Adaptation of the cortical somatosensory evoked potential following pulsed pneumatic stimulation of the lower face in adults. Brain Res 2015;1622:81–90.
[12] Evilsizor MN, Ray-Jones HF, Ellis TW Jr., Lifshitz J, Ziebell JM. Microglia in experimental brain injury: implications on neuronal injury and circuit remodeling. In: Kobeissy FH, editor. Brain neurotrauma: molecular, neuropsychological, and rehabilitation aspects. Boca Raton: CRC Press/Taylor & Francis; 2015.
[13] Hirano M, Kubota S, Koizume Y, Tanaka S, Funase K. Different effects of implicit and explicit motor sequence learning on latency of motor evoked potential evoked by transcranial magnetic stimulation on the primary motor cortex. Front Hum Neurosci 2017;10:671.
[14] Huang Y, Mucke L. Alzheimer mechanisms and therapeutic strategies. Cell 2012;148(6):1204–22.
[15] Kondo R, Saito S, Kuroki A, Sato S, Katakura K, Kayama T. Significance and usefulness of corticospinal motor evoked potential monitoring for lesions adjacent to primary motor cortex. No To Shinkei 2004;56(6):496–502. Japanese.
[16] Li BH, Lohmann JS, Schuler HG, Cronin AJ. Preservation of the cortical somatosensory-evoked potential during dexmedetomidine infusion in rats. Anesth Analg 2003;96(4):1155–60.
[17] Rowed DW, Houlden DA, Basavakumar DG. Somatosensory evoked potential identification of sensorimotor cortex in removal of intracranial neoplasms. Can J Neurol Sci 1997;24(2):116–20.
[18] Son E, Ichida J, Wainger B, Toma J, Rafuse V, Woolf C, et al. Conversion of mouse and human fibroblasts into functional spinal motor neurons. Cell Stem Cell 2011;9(3):205–18.
[19] Zhang ZG, Chopp M. Promoting brain remodeling to aid in stroke recovery. Trends Mol Med 2015;21(9):543–8.
[20] Zvereva ZF, Ravikovich MA, Sovetov AN. The electrophysiological characteristics of the compensatory and restorative processes in the central nervous system of neurosurgical patients in relation to the lateralization of the injury. Patol Fiziol Eksp Ter 1990;(4):22–5. Russian.
[21] Crist RE, Lebedev MA. Multielectrode recording in behaving monkeys. In: Nicolelis MAL, editor. Methods for neural ensemble recordings. Boca Raton: CRC Press; 2008.
[22] McNaughton BL, O'Keefe J, Barnes CA. The stereotrode: a new technique for simultaneous isolation of several single units in the central nervous system from multiple unit records. J Neurosci Methods 1983;8(4):391–7.
[23] Mathiesen C, Caesar K, Akgören N, Lauritzen M. Modification of activity-dependent increases of cerebral blood flow by excitatory synaptic activity and spikes in rat cerebellar cortex. J Physiol 1998;512(Pt 2):555–66.
[24] Henze DA, Borhegyi Z, Csicsvari J, Mamiya A, Harris KD, Buzsáki G. Intracellular features predicted by extracellular recordings in the hippocampus in vivo. J Neurophysiol 2000;84(1):390–400.
[25] Jimbo Y, Robinson HP, Kawana A. Strengthening of synchronized activity by tetanic stimulation in cortical cultures: application of planar electrode arrays. IEEE Trans Biomed Eng 1998;45(11):1297–304.
[26] Khazipov R, Zaynutdinova D, Ogievetsky E, Valeeva G, Mitrukhina O, Manent JB, et al. Atlas of the postnatal rat brain in stereotaxic coordinates. Front Neuroanat 2015;9:161.
[27] Paxinos G, Watson CRR, Emson PC. AChE-stained horizontal sections of the rat brain in stereotaxic coordinates. J Neurosci Methods 1980;3(2):129–49.
[28] Markram H. The human brain project. Sci Am 2012;306(6):50–5.
[29] Abbott A. Neuroscience: solving the brain. Nature 2013;499(7458):272–4.
[30] Underwood E. Brain project draws presidential interest, but mixed reactions. Science 2013;339(6123):1022–3.
[31] Leshner AI. Seize the neuroscience moment. Science 2013;342(6158):533.
[32] Wadman M. Behind the scenes of a brain-mapping moon shot. Nature 2013;495(7439):19.
[33] Benison AM, Rector DM, Barth DS. Hemispheric mapping of secondary somatosensory cortex in the rat. J Neurophysiol 2007;97(1):200–7.
[34] Kimura J. Kugelberg lecture. Principles and pitfalls of nerve conduction studies. Electroencephalogr Clin Neurophysiol Suppl 1999;50:12–5.